UNCLASSIFIED

SECURITY CLASSIFICATION OF THIS PAGE

(2)

AD-A211 599

DTIC ELECTE AUG 21 1989 S B d

REPORT DOCUMENTATION PAGE

Form Approved OMB No. 0704-0188

1a. REPORT SECURITY CLASSIFICATION: Unclaasified	1b. RESTRICTIVE MARKINGS: AFC FILE COPY
2a. SECURITY CLASSIFICATION AUTHORITY:	3. DISTRIBUTION/AVAILABILITY OF REPORT: Approved for public release; distribution is unlimited
2b. DECLASSIFICATION/DOWNGRADING SCHEDULE:	
4. PERFORMING ORGANIZATION REPORT NUMBER(S):	5. MONITORING ORGANIZATION REPORT NUMBER(S): AFOSR-TR-89-1101
6a. NAME OF PERFORMING ORGANIZATION: California Institute of Technology	6b. OFFICE SYMBOL (If applicable):
6c. ADDRESS (City, State, and ZIP Code): 1201 E California Blvd., 252-21 Pasadena, CA 91125	7a. NAME OF MONITORING ORGANIZATION: AFOSR/NA
	7b. ADDRESS (City, State, and ZIP Code): Bolling AFB Washington, DC 20332-6448
8a. NAME OF FUNDING/SPONSORING ORGANIZATION: AFOSR	8b. OFFICE SYMBOL (If applicable): NA
	9. PROCUREMENT INSTRUMENT IDENTIFICATION NUMBER: AFOSR-88-0134
8c. ADDRESS (City, State, and ZIP Code): Bolling Air Force Base Washington, DC 20332-6448	10. SOURCE OF FUNDING NUMBERS: PROGRAM ELEMENT NO. 61102F; PROJECT NO. 2302; TASK NO. C2; WORK UNIT ACCESSION NO.

11. TITLE (Include Security Classification): Stress Wave Induced Damage in Rock

12. PERSONAL AUTHOR(S): Rubin, Allan M and Arhens, Thomas J

13a. TYPE OF REPORT	13b. TIME COVERED	14. DATE OF REPORT (Year, Month, Day)	15. PAGE COUNT
Final	FROM 880415 TO 890314	890601	36

16. SUPPLEMENTARY NOTATION

17. COSATI CODES			18. SUBJECT TERMS (Continue on reverse if necessary and identify by block number)
FIELD	GROUP	SUB-GROUP	Crackings; Damage; Experiments; Rocks; Stress waves

19. ABSTRACT (Continue on reverse if necessary and identify by block number)

Blocks of San Marcos Gabbro and Bedford Limestone were impacted with high-velocity projectiles, and longitudinal elastic velocity measurements were carried out on oriented cubes throughout a cross-section of each block. For both rock types the velocity increases rather uniformly with distance from the impact site, reaching the unshocked velocity at a distance of approximately one crater radius. The maximum observed velocity reduction is to slightly less than half the unshocked seismic velocity for both the gabbro and the limestone. However, the average velocity reduction within the damaged zone is significantly greater for the limestone. Observed anisotropy in velocity reduction in the gabbro sample clearly can be related to the preferred orientation of macroscopic cracks, suggesting that velocity measurements can be a powerful tool for characterizing crack density and orientation in shocked rock. Preliminary microscopic investigation of crack density and orientation confirms this view. Microscopic observations of the gabbro indicate that both the number of cracks per unit area and crack size increase as seismic velocity decreases. Observational estimates of the crack density are generally slightly lower than estimates made from theoretical consideration of the observed velocity reduction.

(continued on ...)

20. DISTRIBUTION/AVAILABILITY OF ABSTRACT	21. ABSTRACT SECURITY CLASSIFICATION
☑ UNCLASSIFIED/UNLIMITED ☐ SAME AS RPT ☐ DTIC USERS	Unclassified

22a. NAME OF RESPONSIBLE INDIVIDUAL	22b. TELEPHONE (Include Area Code)	22c. OFFICE SYMBOL
Spencer T Wu	(202) 767-6962	AFOSR/NA

DD Form 1473, JUN 86 Previous editions are obsolete. SECURITY CLASSIFICATION OF THIS PAGE

UNCLASSIFIED

Microscopic observation of the porous limestone indicate that both the percentage of fractured grains and their degree of comminution increase as seismic velocity decreases. Anisotropy of crack orientation and seismic velocity is less pronounced in the limestone than in the gabbro, possibly because fracture growth is controlled by grain-grain contacts, which tend to be distributed homogeneously. The peak dynamic pressures induced by the quasi-spherical shock waves reached maxima of about 0.97 GPa and 0.84 GPa in the gabbro and limestone, respectively, immediately below the crater floor. Longitudinal elastic wave velocity reduction was restricted to those rock volumes subjected to more than approximately 0.15 GPa dn 0.2 GPa in the gabbro and limestone, respectively.

SECTION 1

INTRODUCTION

The purpose of this project is to understand on a fundamental level the relation of dynamic production of cracks in brittle media, such as rock, to the concurrent reduction in elastic moduli and quasi-static strength. Theoretical work relating crack density and geometry to material modulus reduction (Walsh, 1965; O'Connell and Budiansky, 1974), and more recent work relating crack density to material strength reduction (Sammis and Ashby, 1986; Horaii and Nemat-Nasser, 1986), suggests that it will be possible to obtain a complete and testable theory of shock wave damage in rock. This report describes our initial efforts on this project. It is the first quantitative laboratory study of elastic modulus degradation in shocked rock, and discusses new results concerning anisotropic effects on modulus reduction. The program we have been conducting has had three interrelated concurrent phases.

1) Experimental studies of crack density and modulus reduction produced by hemispherical shock waves in rock. To date this is the most advanced of the three phases. In order to generate a three-dimensional shock wave in rock, blocks of Bedford limestone and San Marcos gabbro were impacted with high-velocity projectiles, and longitudinal elastic wave (P-wave) velocity measurements were carried out on a large number of oriented cubes cut out of each rock sample. Theoretical estimates of seismic velocity reductions based on microscopic observations of crack density are compared to observed velocity reductions for P-waves.

2) Since cracking in the three-dimensional experiments appear to be related to both tensile stress concentration around pores during the compressive pulse, or in response to the tensile portion of the stress wave, in order to better understand the underlying physics of rock failure, we have performed a series of one-dimensional tensile (spall) experiments

on Bedford limestone to characterize the high-strain-rate tensile strength properties of this material. Our strategy was to shock discs of limestone at controlled stress magnitudes and durations below that required to produce complete spalling, and to observe the progression in rock damage. The elastic moduli of the recovered samples were determined by measuring their longitudinal and shear wave velocities. As in the three-dimensional experiments, the seismic velocity deficits can also be used to infer the crack densities that were induced as a function of applied stress and stress duration. Previous impact-induced spall experiments have been conducted at sufficiently high stresses to produce complete one-dimensional tensile failure (Shockey et al., 1974; Grady and Kipp, 1979; Cohn and Ahrens, 1980). Measuring the elastic moduli at arrested stages of tensile failure adds a new dimension to the study of dynamic rock failure because the modulus reduction concurrent with crack growth forms an integral part of models of such failure. Our work has developed a new technique, based on the measurement of the tensile stress required for the onset of a seismic velocity deficit to define the dynamic fracture toughness.

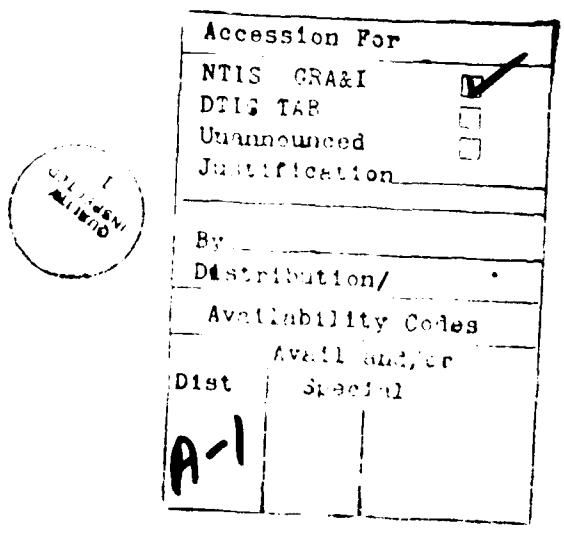

SECTION 2

EXPERIMENTAL - PHASE (1), THREE-DIMENSIONAL EXPERIMENT

a) Sample Preparation

The shocked gabbro specimen is a 20-cm cube of San Marcos Gabbro, a mafic igneous rock with a density of 2.867 g/cm^3 and a very low initial crack density (Lange et al., 1984). It was impacted by a 3.2 mm diameter steel projectile (mass 0.143 g) at a speed of 5.2 km/sec. The resulting crater is approximately 10 cm across and 1.0 cm deep. The upper 5 cm of the specimen was cut in half (Fig. 1) and a 1 cm-thick section was cut from one of the halves. The half of this section corresponding to the left half of Figure 1 was cut into oriented ~1-cm cubes for P-wave velocity measurements.

The shocked limestone specimen is a block of Bedford Limestone 20 cm on a side and 12 cm deep. The rock has a bulk density of 2.62 g/cm^3, an average grain size of approximately 0.5 mm, and a pore porosity of approximately 0.12. It was impacted by a 5.6 mm diameter copper-jacketed lead bullet (mass 3.2 g) at a speed of 1.2 km/sec. The upper 6.8 cm of the sample was cut in half in order to prepare oriented cubes as for the gabbro.

The ~1 cm cubes from both samples were dried in an evacuated oven at 100° C until further weight loss over a twelve-hour period was less than 10^{-4} g, and seismic velocities were measured at 0.4 MHz. The P-wave velocity, C_p, of the unshocked gabbro and limestone were determined to be approximately 6.4 ± 0.2 km/sec and 3.9 ± 0.1 km/sec, respectively. We assume the 1 cm^3 samples are representative of the rock in bulk; that is, we believe no further crack damage was done upon sawing and in preparing the samples for ultrasonic measurements. These assumptions need to be tested by further work (for example, by preparing samples of different sizes, using different sawing techniques, changing the frequencies at which the elastic moduli are probed, etc.).

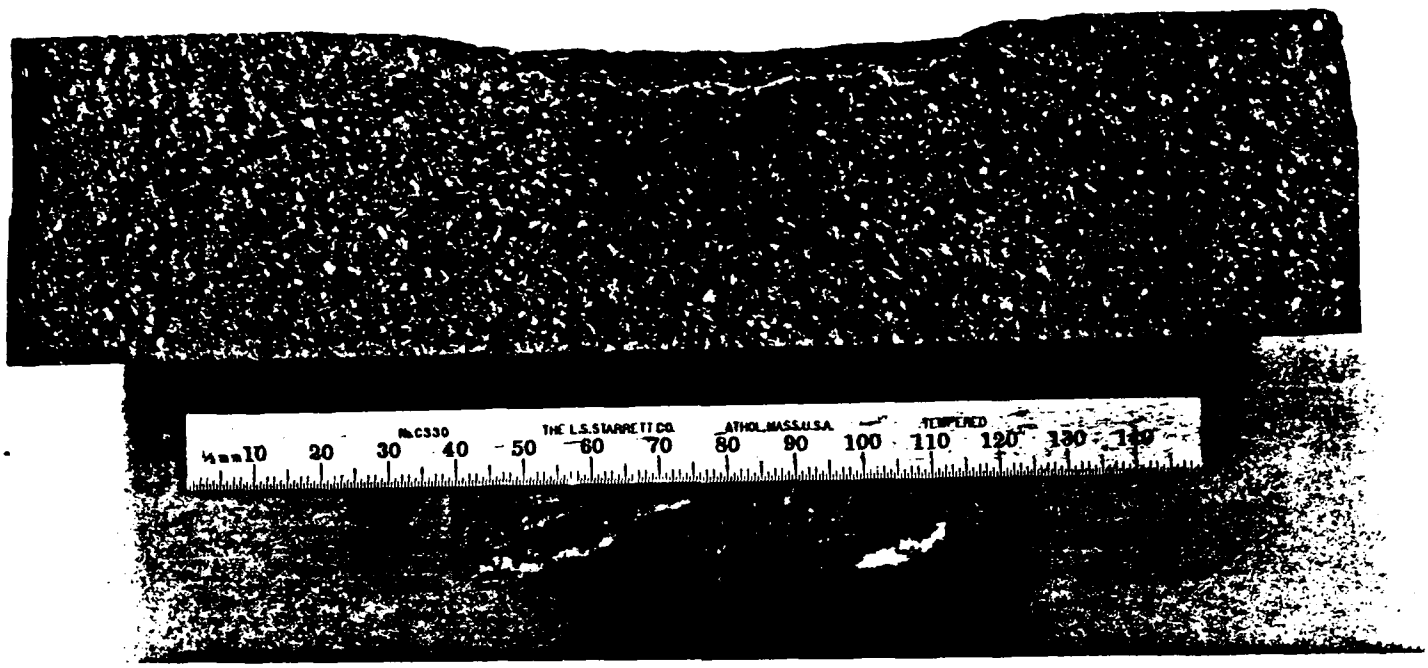

Figure 1. Cross-section of shocked San Marcos Gabbro cut through a crater diameter. Projectile was fired vertically downward upon upper surface (at approximately the 80 mm mark). Measurements were made on the other half of the sample corresponding to the left half of the figure. Cracks are highlighted by water-soluble saw coolant. The crack density near the impact site is great enough that individual cracks cannot be distinguished in this photograph.

TJA89020SG

b) Velocity Measurements

San Marcos Gabbro

The results of the velocity measurements on gabbro are shown in Figure 2. z is taken parallel to the impact direction, x perpendicular to the impact direction in the plane of the cross-section, and y out of the plane of the cross-section. The directional P-wave velocities C_p are plotted as a function of distance from the impact axis (z) for various depths within the sample. The velocity reductions appear to be systematic, and the following generalizations can be made:

(1) With the exception of a single sample, all longitudinal elastic (P-wave) velocity measurements are greater than 0.6 times the unshocked velocity.

(2) For each depth within the sample, the velocity increases as a function of horizontal distance from the impact, reaching typical unshocked velocities at distances approximately equal to or slightly greater than the crater radius (5 cm).

(3) Beneath the crater, velocity increases with depth, reaching values 0.85 of the unshocked velocity at the base of the specimen directly beneath the impact.

(4) The samples exhibit locally pronounced seismic anisotropy. The anisotropy is greatest in the upper left part of the specimen, where major vertical fractures associated with the specimen edge can be observed (Figure 1). Such fractures are expected to reduce the crack-perpendicular (x) velocity much more than the crack-parallel (z, y) velocities (Anderson et al., 1974), which is the observed result (Figure 3). The reduced z velocities at the 1.5 cm depth are most likely due to the sub-horizontal cracks associated with reflections off the free surface (Figs. 1,3).

Elsewhere within the specimen, the anisotropy is less pronounced but still apparent. Figure 3 illustrates the P-wave velocity in the x, y, and z directions at 2.5 cm depth within the sample. Within the central portion of the crater the vertical (z) velocity is slightly but consistently less than both horizontal (x, y) velocities. This is consistent with the large

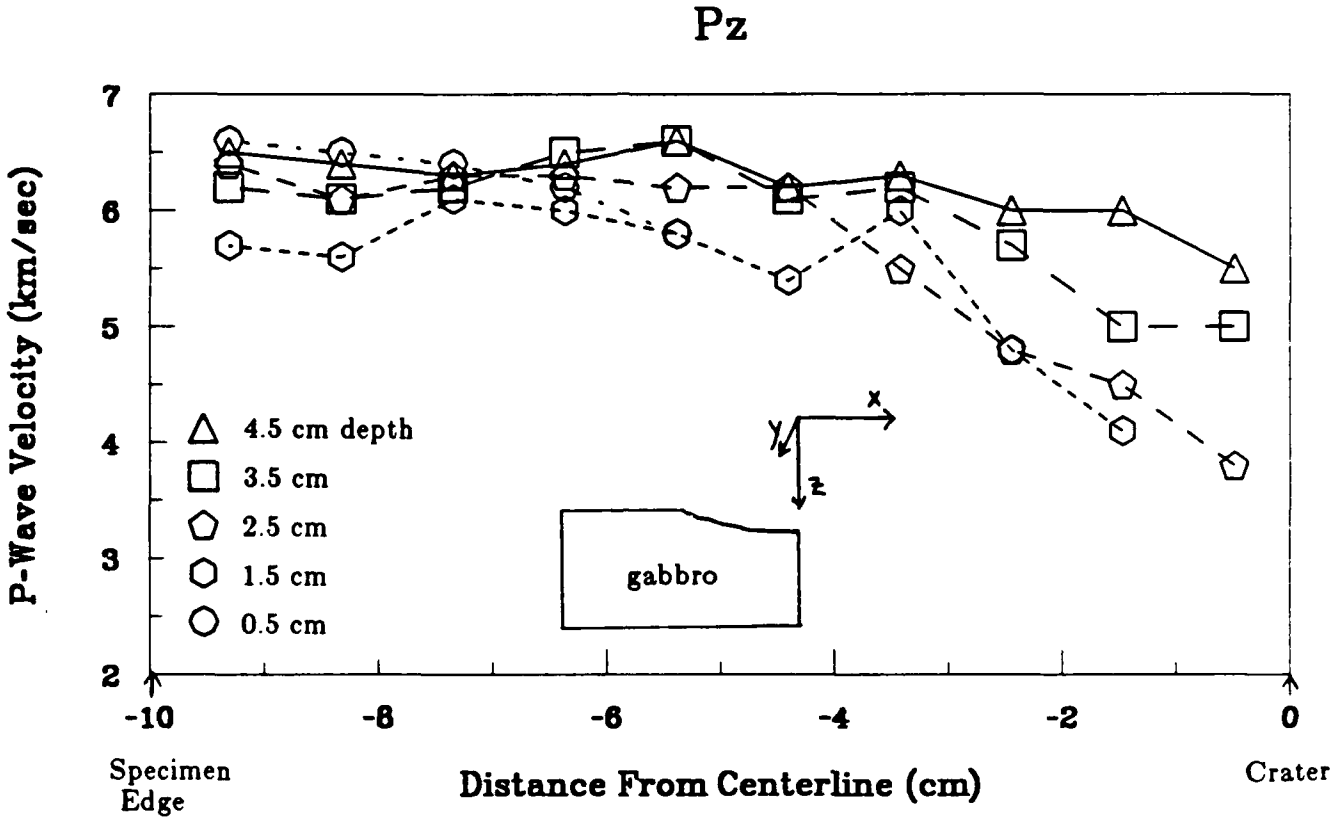

Figure 2. P-wave velocities for gabbro as a function of distance from the *z* axis (projectile path), at indicated depths within the sample. Deepest velocities are generally the highest, near the impact site. Pz, velocity in *z* direction; Px, velocity in x direction; Py, velocity in y direction (see sketches).

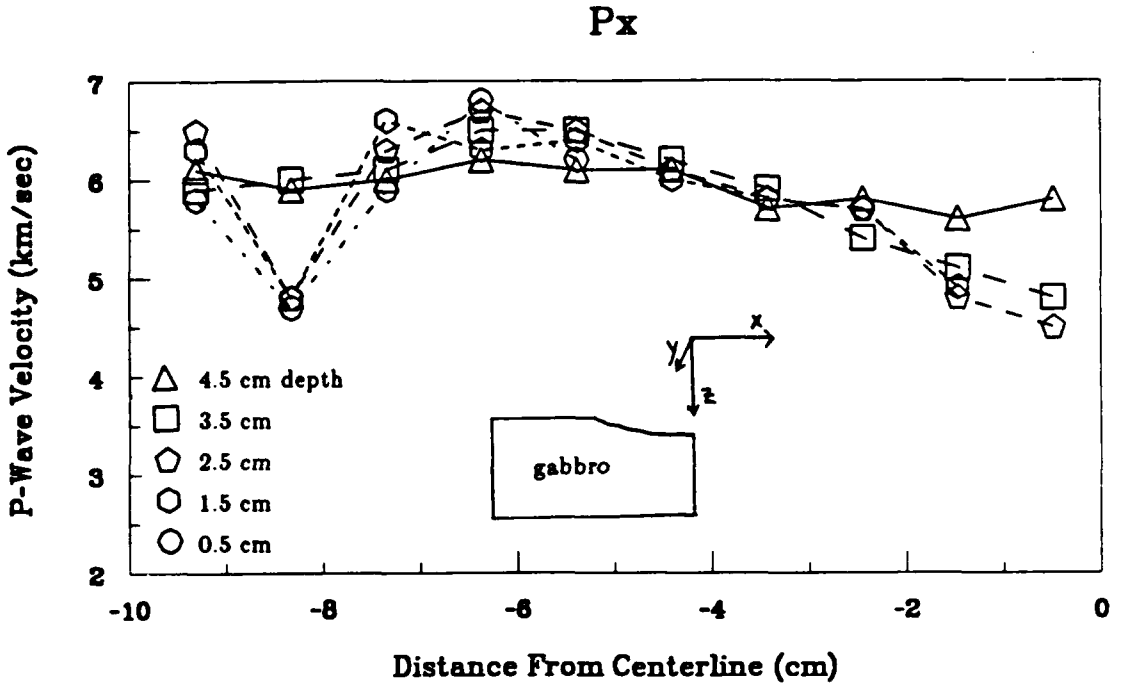

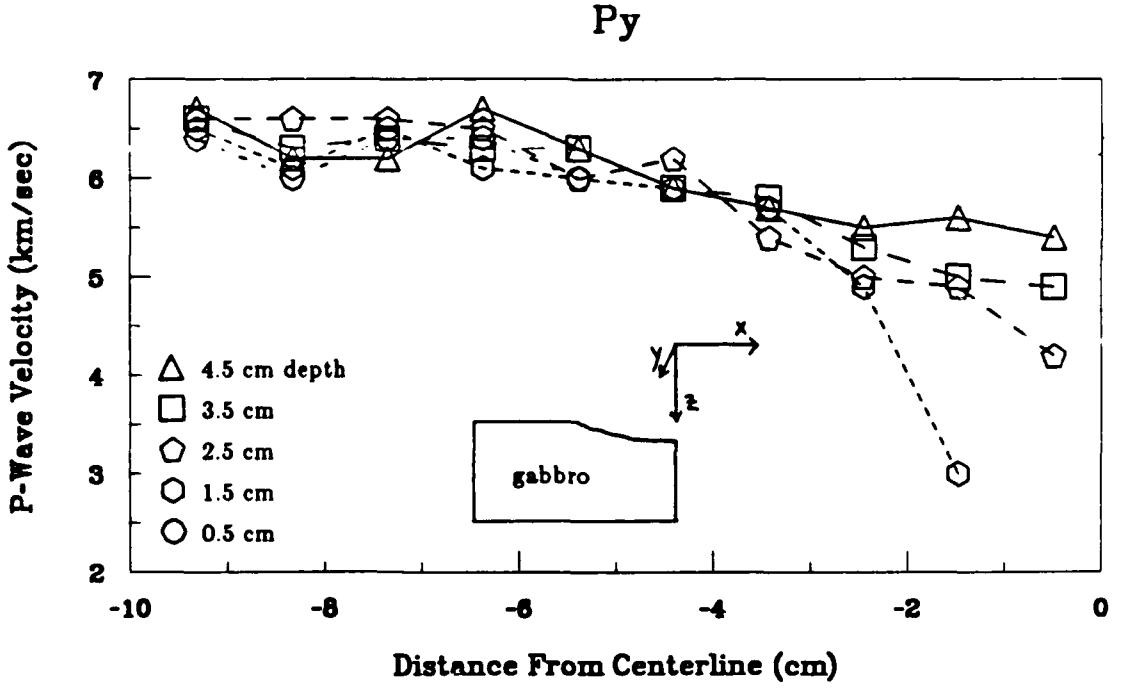

Figure 2 continued

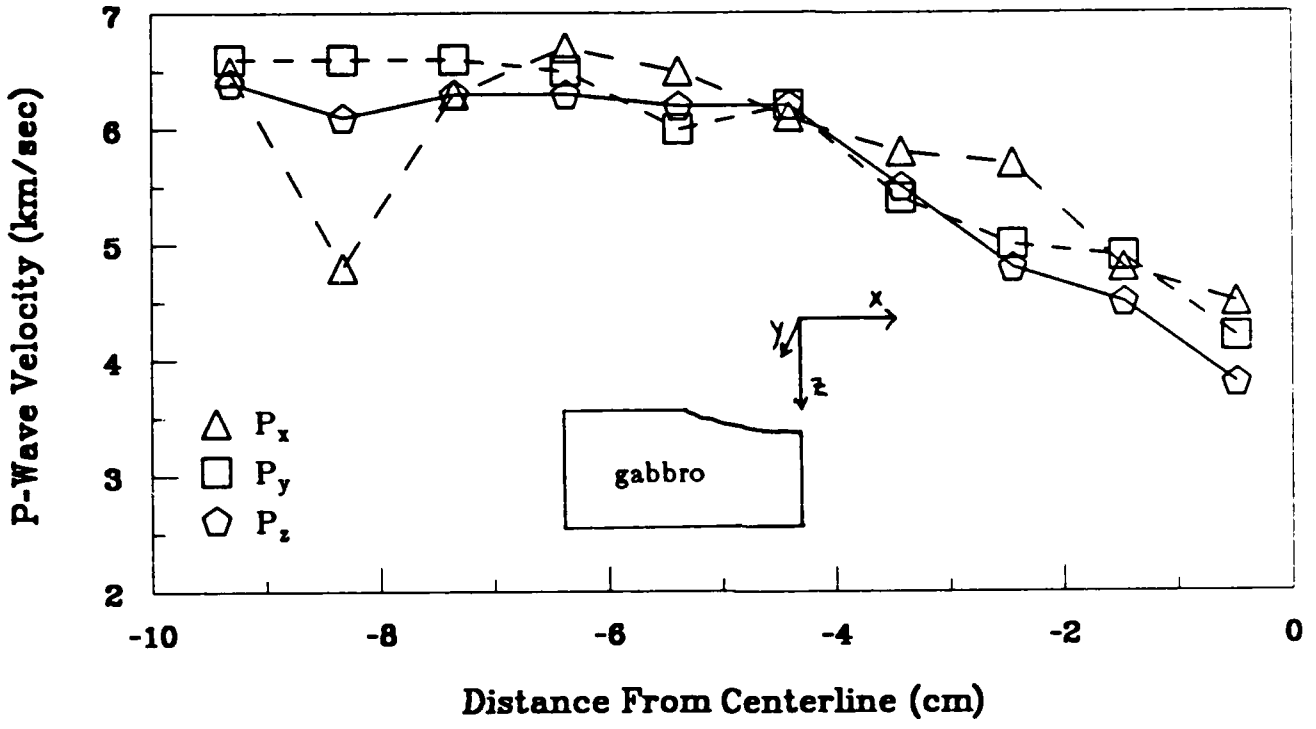

Figure 3. P-wave velocities for gabbro in x, y, and z directions at 2.5 cm depth below the surface. The pronounced anisotropy near the sample edge is due to the oriented macroscopic cracks visible in Fig. 1. It also appears that the z direction is slowest of the three beneath the crater, but reaches its far-field velocity at lesser distances than the x and y directions.

sub-horizontal cracks somewhat concentric with the crater floor (Fig. 1). In addition from Figures 2 and 3 it appears that, with the exception of the sample located at a depth of 1.5 cm, the vertical (z) P-wave velocity approaches unshocked values at lesser radial distances than do the horizontal (x,y) velocities (approximately 4.5 cm as opposed to 6.5 cm). The 1.5 cm depth layer includes the large sub-horizontal cracks outside the crater region in Fig. 1. Because the observed anisotropy is relatively slight, additional samples should be shocked and measured to corroborate this result.

Figure 4 shows all the velocity measurements as a function of radial distance from the assumed effective center of the approximately spherical stress wave emanating from the impact. In this study it is taken to be located along the impact axis at a depth equal to 1/2 the crater depth. The tendency for the seismic velocity to increase smoothly to its unshocked value at a radial distance of approximately one crater radius is apparent. The average velocity in the vicinity of the crater floor is approximately 0.65 times the unshocked velocity.

Bedford Limestone

The results of the velocity measurements on limestone are shown in Figures 5 and 6. In many respects the measurements resemble those made on the gabbro. For instance:

(1) The greatest reduction in seismic velocity, occurring just beneath the crater floor, is to values slightly less than half the unshocked value. The maximum velocity reduction is slightly greater for the limestone (0.41 times the unshocked value) than for the gabbro (0.47 times the unshocked value).

(2) For each depth interval within the sample, the velocity increases as a function of horizontal distance from the impact.

(3) Beneath the crater floor, the velocity increases monotonically with depth. Away from the crater, this is not the case. At these distances, the depth interval immediately below the crater floor possesses the lowest velocities (in the z and y

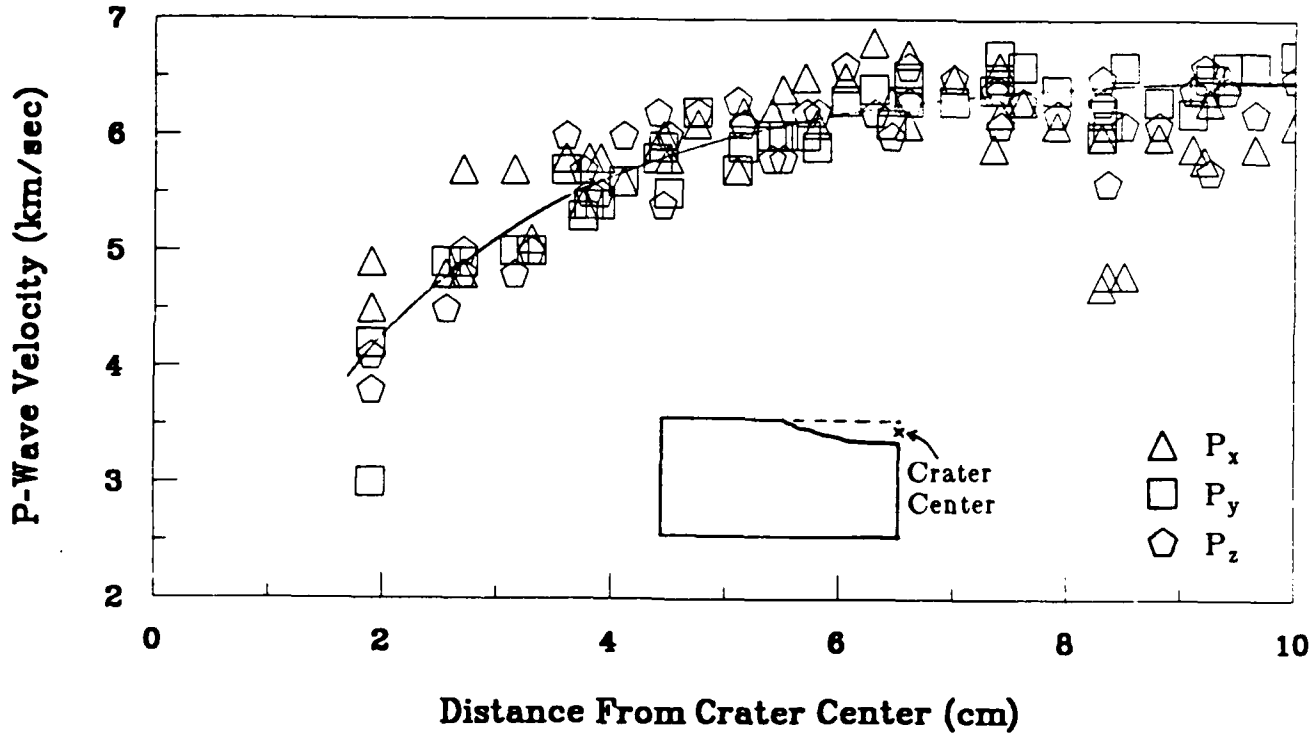

Figure 4. Plot of all velocity measurements for gabbro as a function of distance from the crater center. Curve is eyeball fit to data.

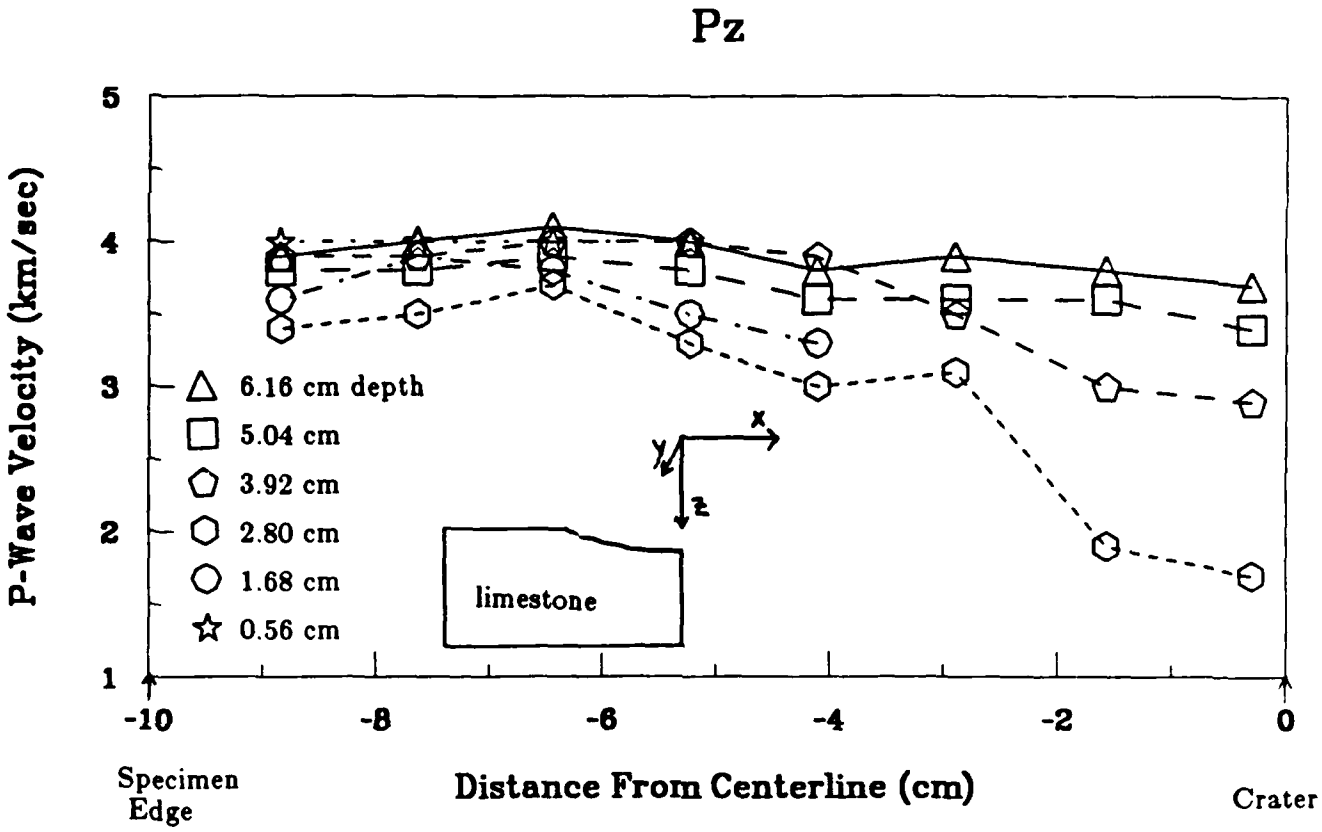

Figure 5. P-wave velocities for Bedford limestone as a function of distance from the z axis (projectile path), at indicated depths within the sample. Deepest velocities are generally the highest, near the impact site. Pz, velocity in z direction; Px, velocity in x direction; Py, velocity in y direction (see sketches).

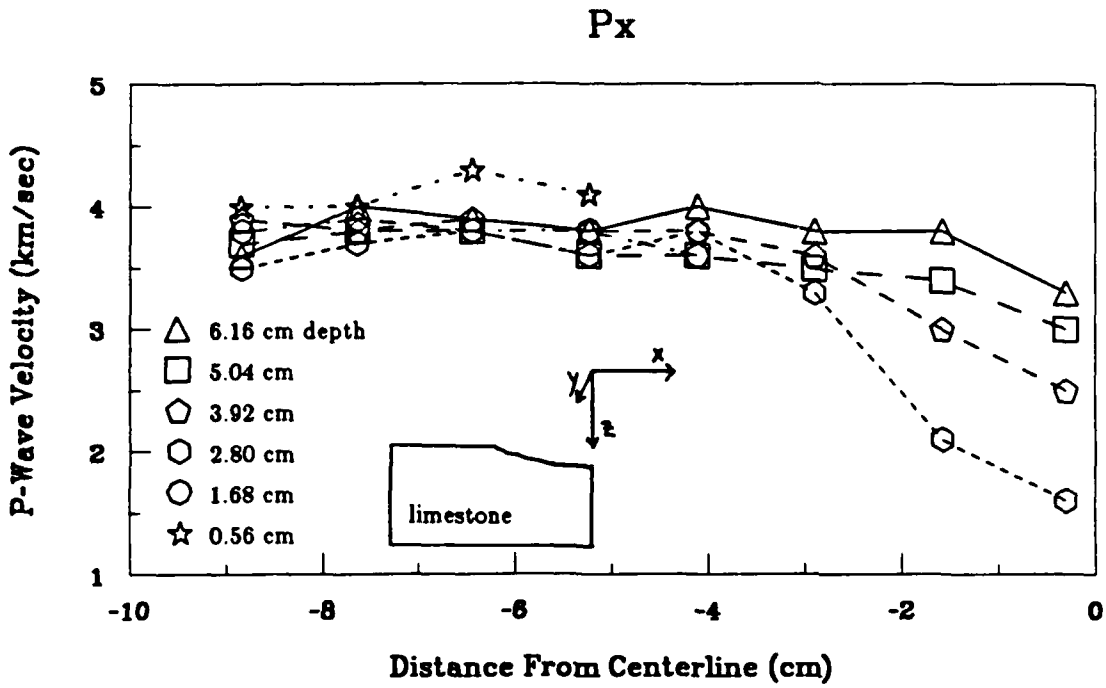

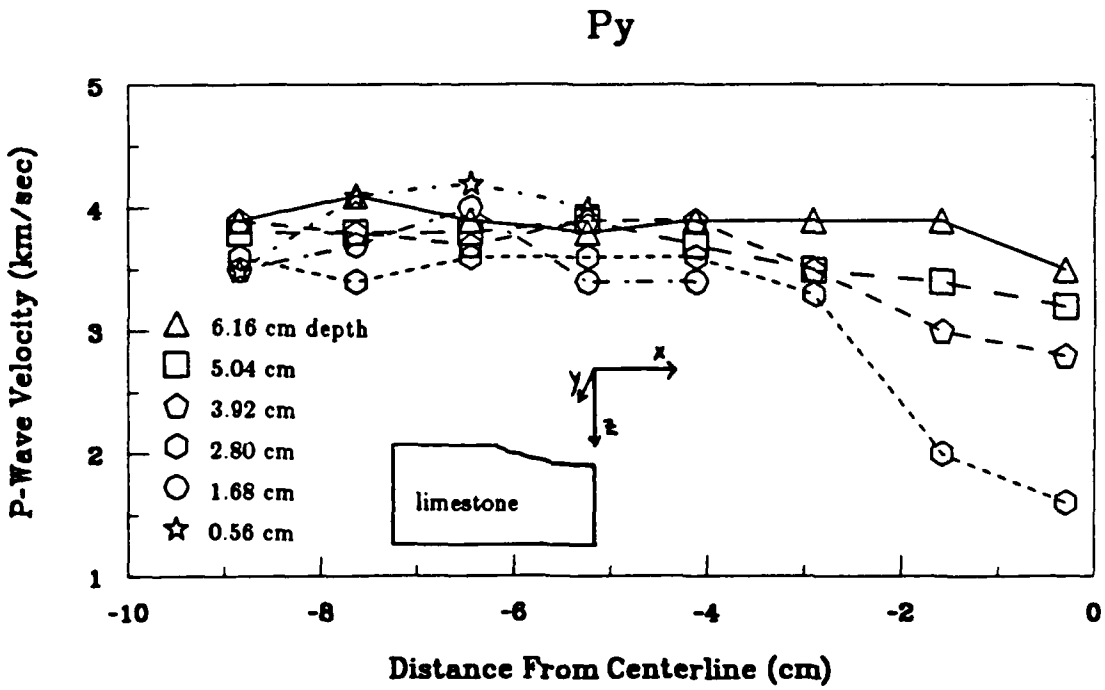

Figure 5 continued

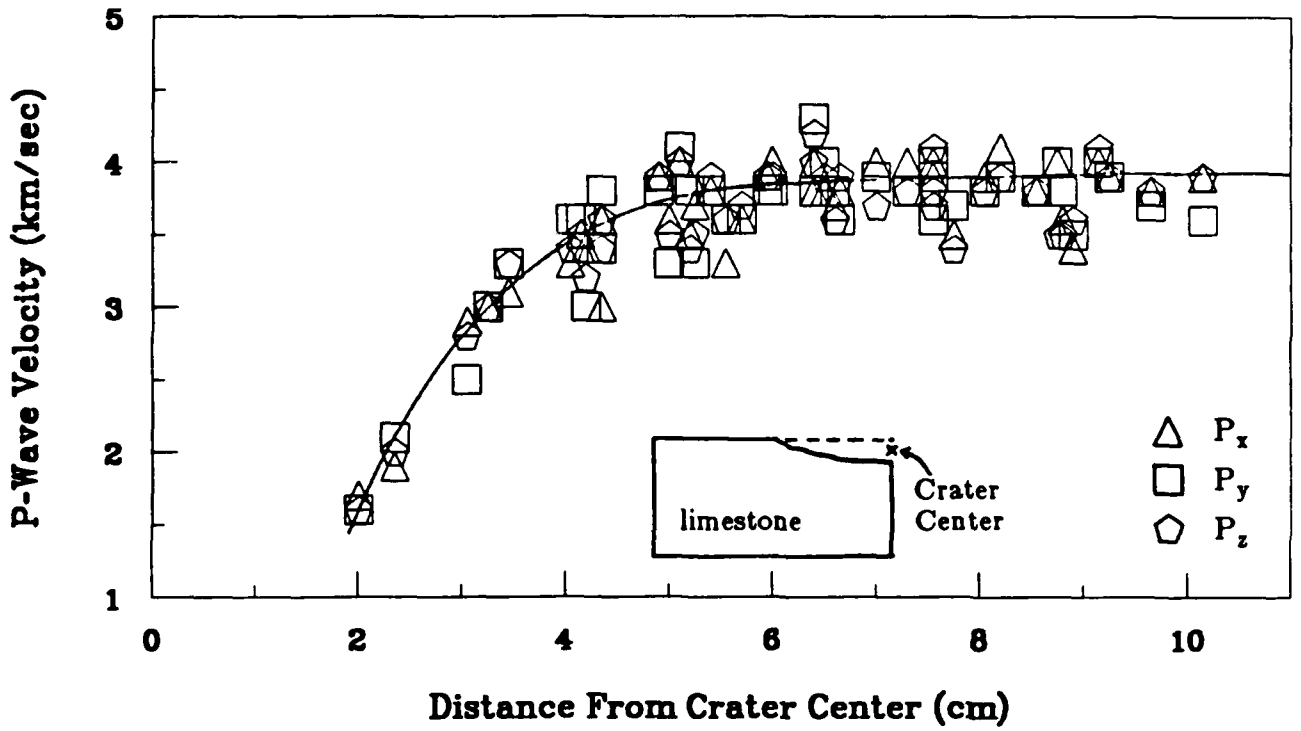

Figure 6. Plot of all velocity measurements for limestone as a function of distance from the crater center. Curve is eyeball fit to data.

directions), and velocity increases toward both the top and bottom of the sample. This low-velocity interval includes the only macroscopic spall fractures within the sample.

(4) Seismic anisotropy within the limestone, if present, is much less than within the gabbro. This is particularly evident nearest the crater center, where the scatter in velocity for the limestone (Figure 6) is strikingly less than for the gabbro (Figure 4).

(5) As seen in Figure 6, the velocities increase relatively smoothly with distance from the crater center. The average of the velocity reductions at a given radial distance is significantly greater within the limestone than within the gabbro. The seismic velocity approaches its unshocked value at a slightly lesser distance, relative to the crater radius, in the limestone than in the gabbro.

c) Correlation with Crack Density

San Marcos Gabbro

Comparison of Figure 1 with Figures 2 and 4 indicates that the zones of greatest velocity reduction correspond closely to the zones of greatest crack concentration. Within the dark central region in Figure 1, with a radius of about 3.5 cm, where cracks are too numerous to detect individually at this scale, velocities are less than 0.83 of the unshocked velocity (5.3 km/sec). Within the highly fractured region between about 3.5 and 5.5 cm from the equivalent center, velocities increase to about 0.94 of the unshocked value (6.0 km/sec).

Microscopic observation of the 1-cm cubes at 25x indicates cracks ranging from grain boundary cracks and cleavage cracks internal to plagioclase and amphibole (0.1-1 mm) to cracks which apparently traverse the entire cube. Cleavage cracks and grain-crossing cracks are restricted largely to highly-shocked low-velocity samples near the impact. Both crack density and maximum crack length increase as seismic velocity decreases. Thus samples with relatively high velocities far from the impact have about 1 crack of average length 0.5 mm per mm of traverse, while samples close to the impact have

as many as 2.3 cracks of average length 1.2 mm per mm of traverse. Crack anisotropy is also apparent at this scale. For example, in some cubes below the crater floor with lowest velocities in the vertical (z) direction, the density of (sub-horizontal) cracks intersecting a vertical traverse is very high, while the density of (sub-vertical) cracks intersecting a horizontal traverse is no greater than that in cubes far away (although the average crack length is greater).

Existing theories relating seismic velocity reduction to crack density assume either that the cracks are randomly oriented (e.g., O'Connell and Budiansky, 1974), or uniformly aligned (e.g., Anderson et al., 1974). The cracks within the cubes cut from the shocked gabbro have preferred but non-uniform orientations, and are therefore an intermediate case to those modeled theoretically. The important crack-density parameter in these studies is $\varepsilon = N \langle c^3 \rangle$, where N is the number of cracks per unit volume and $\langle c^3 \rangle$ is the average of the cube of the characteristic linear dimension (half-length) of the crack (O'Connell and Budiansky, 1974, eq. 4). Because of the c^3 term the influence on velocity is heavily weighted toward the largest cracks present. Using a relation given by O'Connell and Budiansky (1974), ε is related to the observed crack trace density approximately as

$$\varepsilon = \frac{3}{4\pi} M \langle l^2 \rangle, \qquad (1)$$

where M is the number of line segments per unit area, and l is the segment length. Optical estimates of ε were made on 9 cubes at various distances from the crater center. Independent estimates were obtained for each of the x, y, and z directions, based on the number and lengths of cracks with length greater than 0.4 mm crossed by oriented traverses. Usually, though not always, the direction producing the highest value of ε was the direction of lowest longitudinal wave velocity in the sample. Estimates of ε ranged from 0.01 near the specimen edge to 0.28 just beneath the crater. The range of directional values of ε within a single sample were typically considerably greater than the observed

range of seismic velocity measurements for the sample. In the most extreme case, the sample with the highest value ($\varepsilon = 0.28$) produced an estimate of only ε=0.04 in the direction of highest velocity, not much greater than in samples far from the impact. The variation in seismic velocity within the sample was only a factor of 1.2, as opposed the factor of 7 variation in ε. The *largest* value of ε is plotted for each sample in Figure 5.

Accepting the O'Connell and Budiansky (random orientation) theory at face value, ε can be computed from the reduction in P-wave velocity using the following equations:

$$\frac{\bar{K}}{K} = 1 - \frac{16}{9}\left(\frac{1-\bar{\upsilon}^2}{1-2\bar{\upsilon}}\right)\varepsilon \qquad (2)$$

$$\bar{\upsilon} = \upsilon\left(1 - \frac{16}{9}\varepsilon\right) \qquad (3)$$

$$\frac{\overline{C_p}}{C_p} = \left(\frac{(1-\bar{\upsilon})(1+\upsilon)}{(1+\bar{\upsilon})(1-\upsilon)}\frac{\bar{K}}{K}\right)^{1/2} \qquad (4)$$

where K is bulk modulus, υ is Poisson's ratio, and bars denote effective values appropriate for the cracked body. The values of ε that would reproduce the fit to the velocity data in Figure 4 are shown in Figure 7, together with the values determined optically. An initial crack density ε of 0.0 (for practical purposes equal to the lowest observed value of 0.01) was assumed. The computed values of ε are up to a few tens of percent greater than the observed values. The computed value of ε producing the maximum P-wave velocity reduction of 50% is 0.4, as opposed to the observed value of 0.28. This discrepancy could be due in part to the neglect of cracks less than 0.4 mm in length. Further observation at higher power is required to determine if this is the case. In addition, the maximum observed value of ε for each sample produces a considerably better fit to the average velocity than does the average ε (put another way, the lowest observed value of ε produces a very poor estimate of the highest velocity in each sample). Thus the existing theory of O'Connell and Budiansky (1974), which assumes random crack orientation, cannot be

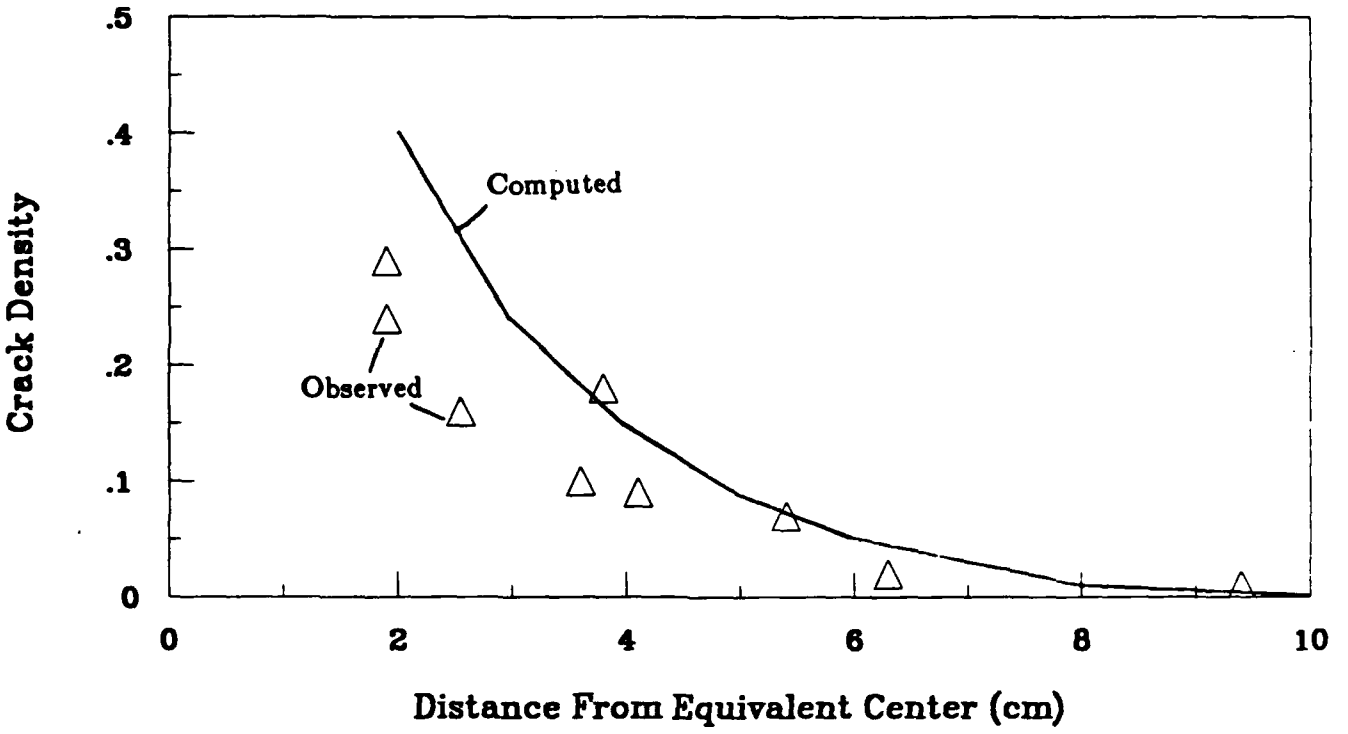

Figure 7. Plot of maximum observational estimate of e for each gabbro sample measured (triangles), as a function of distance from the crater center. Also shown is the computed plot of e versus distance, using the theory of O'Connell and Budiansky (1974) and the fit to the velocity data from Figure 4 (solid line).

used in this simplified fashion to describe the directional properties of the velocity measurements in detail. Further microscope observation, shear wave velocity measurements, and consideration of aligned-crack models are necessary to determine if refinements of the theoretical models relating crack density to modulus reduction in shocked rock are required.

Bedford Limestone

Preliminary observation of the crack density in the limestone at 50x indicates that both the percentage of fractured grains and their degree of comminution decreases rapidly away from the crater center. In the closest region, about 2 cm distant, nearly all the grains are severely fractured and shattered. A short distance further about half the grains are fractured, with from 1 to about 10 cracks each. By about 3 cm distant, only about 5% of the grains contain visible fractures, although the velocity reduction is still pronounced. From this observation it seems likely that the initial stage of inelastic failure involves fracture along grain boundaries. Grain/grain contacts tended to be eroded by the polishing process and therefore grain boundary cracks could not be observed with the technique used. The importance of grain/grain contacts in initiating crack growth, and their homogeneous distribution within the limestone, could explain the apparent lack of anisotropy of the velocity measurements.

d) Correlation with Peak Dynamic Pressure

Most of the highly shocked region not ejected during crater formation lies within the "pressure decay regime" of Ahrens and O'Keefe (1987). Within this regime, the peak dynamic pressure decays as $(1/r)^n$, where r is distance. n is 1.70 for an impact velocity of 5.2 km/sec (the velocity of the gabbro impactor) and 1.30 for an impact velocity of 1.2 km/sec (the velocity of the limestone impactor) (Ahrens and O'Keefe, 1987, eq. 8). Within the "impedance match regime" of Ahrens and O'Keefe, which extends several projectile

radii into the sample, the peak dynamic pressure is nearly constant. We approximate the distance r within the pressure decay regime as being equal to the distance from the crater center. Then the peak dynamic pressure is given approximately by:

$$P = \frac{\rho_T \rho_P C_p^T C_p^P}{\rho_T C_p^T + \rho_P C_p^P} U\left(\frac{a}{r}\right)^n \qquad (5)$$

where C_p^T and C_p^P are the target and projectile longitudinal wave velocities, respectively, and U is impact velocity. The peak dynamic pressures within the gabbro and limestone are plotted as a function of distance from the crater centers in Figures 8 and 9. The most highly shocked regions recovered from the gabbro, with seismic velocities from about 0.45 to 0.75 times that of unshocked rock, experienced a peak pressure of approximately 0.97 GPa.

e) Conclusions

The seismic velocities of the shocked sample are indistinguishable from those of unshocked gabbro below a peak pressure of about 0.15 GPa. The pressure within the impedance match regime was lower for the limestone because of the lower projectile velocity, but decayed less rapidly with distance because of the lower value of n and the greater projectile radius. The most highly shocked regions recovered from the limestone, with seismic velocities of about 0.41 times that of unshocked rock, experienced a peak pressure of approximately 0.84 GPa (Fig. 9). The seismic velocities are indistinguishable from those of unshocked rock for those volumes subjected to pressures less than 0.2 GPa. Greater attenuation within the limestone than the gabbro could make this low-pressure limit an overestimate.

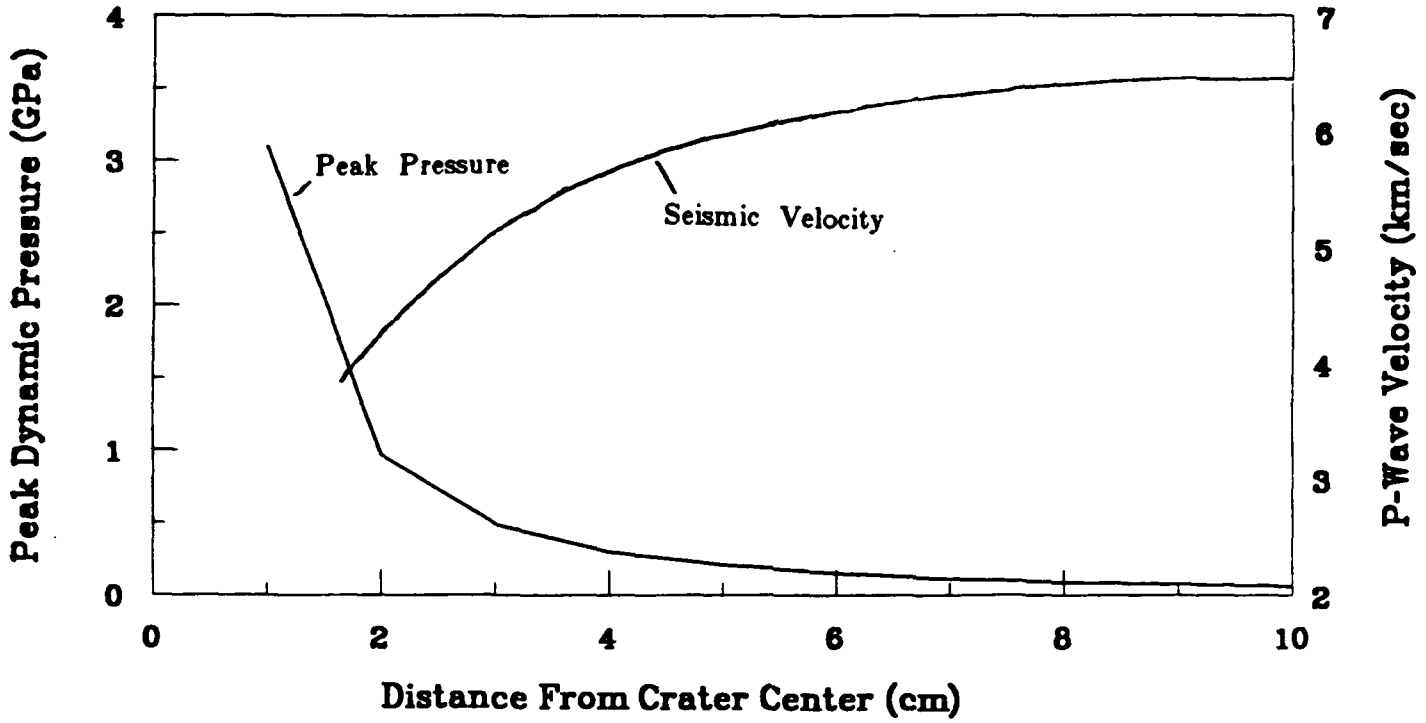

Figure 8. Plot of computed peak dynamic pressure within the gabbro as a function of distance from the crater center, along with fit to velocity data from Fig. 5.

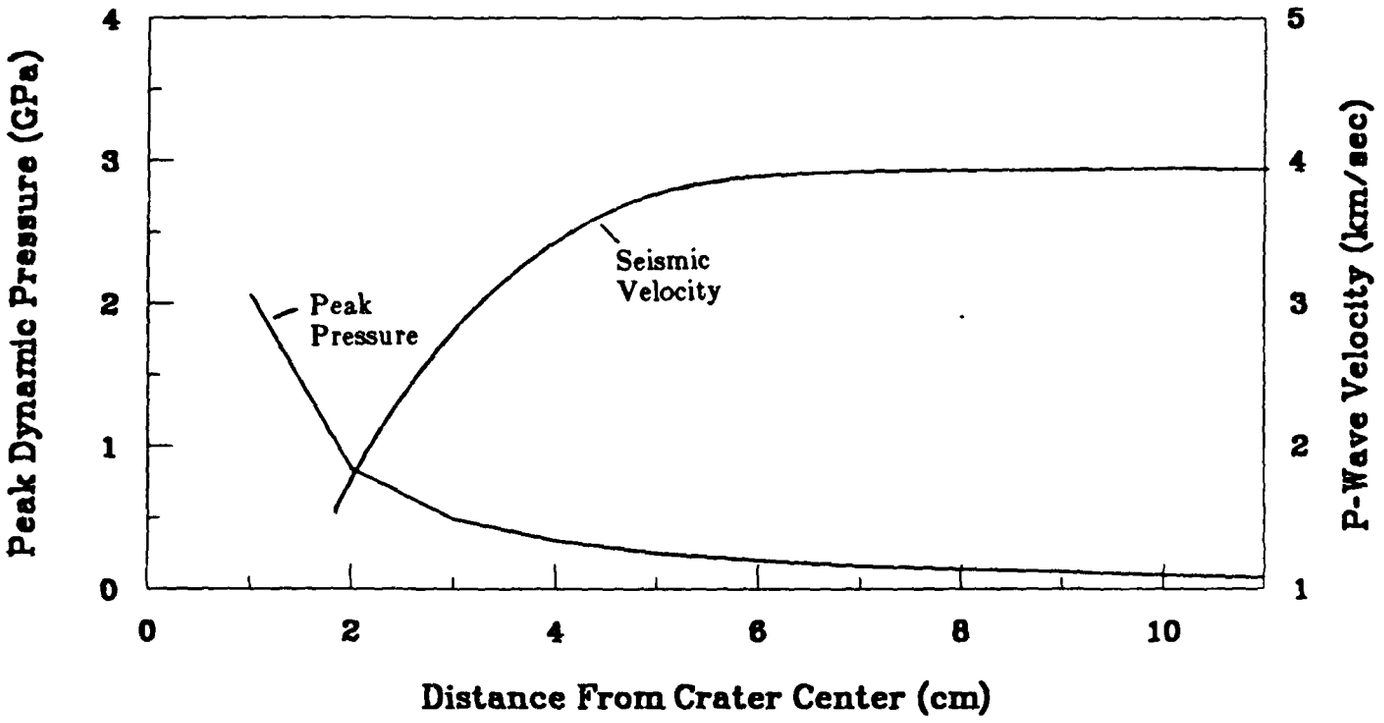

Figure 9. Plot of computed peak dynamic pressure within limestone as a function of distance from the crater center, along with fit to velocity data from Fig. 3.

Although there is a clear inverse correlation between peak dynamic pressure and seismic velocity, because rock is considerably weaker in tension than compression, it is expected that some cracking takes place in the tensile stress pulse that follows the peak compression. In addition, consideration of the peak pressure alone, derived from hydrodynamic models assuming isotropic pressure at a point, cannot adequately account for the growth of cracks in a region undergoing macroscopic compression, or crack anisotropy. In order to provide a more detailed explanation of the distribution and orientation of fractures, more detailed analyses of the stress field resulting from impact are required, and we intend to carry this out. It is noteworthy that the shallow, sub-horizontal cracks dipping slightly away from the crater floor in Figure 1 match rather closely the theoretical spall surface calculated by Lange et al. (1984). Experiments such as these provide important guides for the development of more refined theoretical descriptions of shock-induced damage in rock.

SECTION 3

EXPERIMENTAL - PHASE (2), ONE-DIMENSIONAL TENSIONAL TESTS

a) Experimental

The muzzle area and recovery tank of the 40 mm gun facility in the Seismological Laboratory at Caltech are illustrated in Figure 10. A Lexan projectile with an aluminum or PMMA flyer plate is accelerated down the gun barrel using a compressed air breach to achieve controlled velocities of 10-30 m/s. The velocity is obtained from timing lasers near the target. The flyer plate impacts the surface of the rock sample, which then flies free into the target trap. The sample, approximately 2.5 cm in diameter and 0.75 cm thick, is polished so that its front and rear faces are flat and parallel to within 0.005 mm, and is carefully aligned to ensure planar impact. Upon impact, compressive waves propagate forward into the target and back into the flyer plate (Figure 11, 0.36 μs). Tension is produced within the sample when the tensile waves due to reflections from these compressive waves at the rear faces of the target and flyer plate meet within the sample (Figure 10, 1.59 μs).

The magnitude of compressive stress within the sample is derived from the equations of conservation of mass and momentum across the shock front, which together give

$$\sigma_t = \frac{\rho_i c_i \rho_t c_t}{\rho_i c_i + \rho_t c_t} U_i, \qquad (6)$$

where ρ is density, c is shock velocity, the subscripts i and t refer to the flyer plate (impactor) and target, respectively, and U_i is the projectile impact velocity (Cohn and Ahrens, 1980). The stress magnitude is therefore controlled by varying the projectile

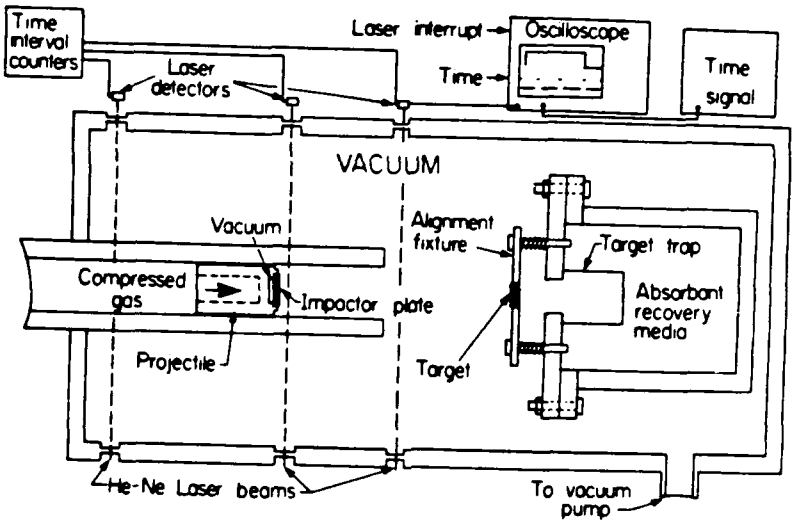

Figure 10. Sketch of muzzle area of gas gun showing recovery tank, sample holder, and alignment fixture. The velocity of the projectile is determined both by the travel time between laser beams and by the duration of the interruption of the third beam by the projectile. After impact the sample breaks its supports and flies freely into the target trap, . where it is protected from further damage.

velocity. Several assumptions are made in equating this compressive stress with the tensile stress achieved following reflection and superposition of the stress waves. First, it is assumed that the shock wave velocities at these moderately low stresses (several tens to over 100 MPa) are equal to the ultrasonic velocities. Cohn and Ahrens (1980) showed that because of the low value of ρ_C for PMMA compared to rock, a 10% increase in c_t corresponds to less than a 2% increase in σ_t, and for aluminum, the increase is less than 6%. Second, because of the greater strength of rock in compression than tension, it is assumed that no damage or wave attenuation occurs during the initial compressive pulse. Third, it is assumed that the velocity of the reflected tensile pulse (rarefaction wave) is the same as that of the incident compressive wave. This allows the stress pulse durations to be computed from the material ultrasonic longitudinal-wave velocities. For the case illustrated in Figure 10, the flyer plate thickness is chosen so that the reflected tensile pulses meet at the sample center. This was the geometry used in the PMMA flyer-plate experiments. In this case, tension is first introduced when the stress wave has traversed 1.5 times the sample thickness, and ends (if spalling does not occur) when the stress wave has traversed 2.5 times the sample thickness. If the flyer plate is thinner or made from a material with a greater longitudinal wave velocity, then tension is first introduced at a location between the rear surface of the sample and the sample center, and [illegible] orter duration, the duration now being the time required for the stress wave to traverse twice the flyer plate thickness (equivalent to the situation in Figure 11 but with the rear surface of the sample displaced further from the impact plane). This was the geometry used in the aluminum flyer-plate experiments. Fourth, it is assumed that the experiments are one-dimensional; that is, that the sample edges are sufficiently far from the center that information has not propagated from them to the sample center prior to the cessation of tension. Strictly speaking this requires diameter-to-thickness ratios of from 4 to 5, depending upon the geometry of the experiment, but in the current experiments a ratio of

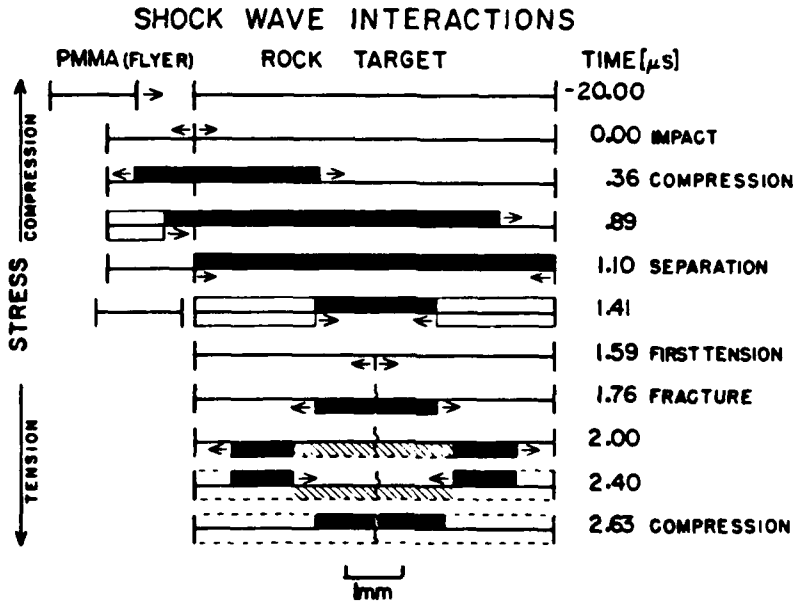

Figure 11. Diagrammatic representation of sequence of 11 states produced upon interaction of shock waves developed at impact. In the diagram encompassing both target and impactor the vertical direction represents stress. Initial compressional waves propagate away from the impact plane, are reflected from the free surfaces of the target and impactor plate, and then superimposed in the middle of the target to create uniaxial extension with ~1-ms duration. The timing of the events depicted depends on the wave velocity and thickness of the target and impactor plate, while the stress level is controlled by the material impedances and impact velocity.

3.3 was used in order to suppress radial cracking of the sample. Thus the tensile strain is one-dimensional during the early stages but not the later stages of tension.

Finally, it is assumed that the magnitude of the reflected tensile pulse is that of the compressive pulse impacting the rear surface of the sample. However, because the pulse has a finite rise time, if crack growth initiates before the peak stress is reached, the pulse may be attenuated before reaching the magnitude of the incident compressive wave. This effect is presumably insignificant at stresses below that at which cracking is introduced (detected from the velocity reduction of the recovered samples), but will become more important as the spall strength is reached. In the future we will determine the tensile stress history within the sample at selected impact velocities using a displacement interferometer (Grady and Kipp, 1979) to test this assumption.

b) A New Method for Measuring Fracture Toughness

The results of the ultrasonic velocity measurements on the recovered targets are shown in Figure 12. Both longitudinal-wave and shear-wave velocities were measured. Important points are:

(1) Tensile failure occurs at computed stresses of about 180 MPa for the shorter duration (0.5 μs) aluminum flyer-plate experiments, much higher than the 70 MPa computed for the longer-duration (1.2 μs) PMMA flyer-plate experiments.

(2) In the shorter-duration experiments, velocity reductions increase nearly linearly over a wide range of peak stresses less than the ultimate tensile strength, whereas in the longer-duration experiments, velocity reductions at stresses less than the ultimate tensile strength occur over a much narrower interval, are less consistent, and appear to be lower in magnitude.

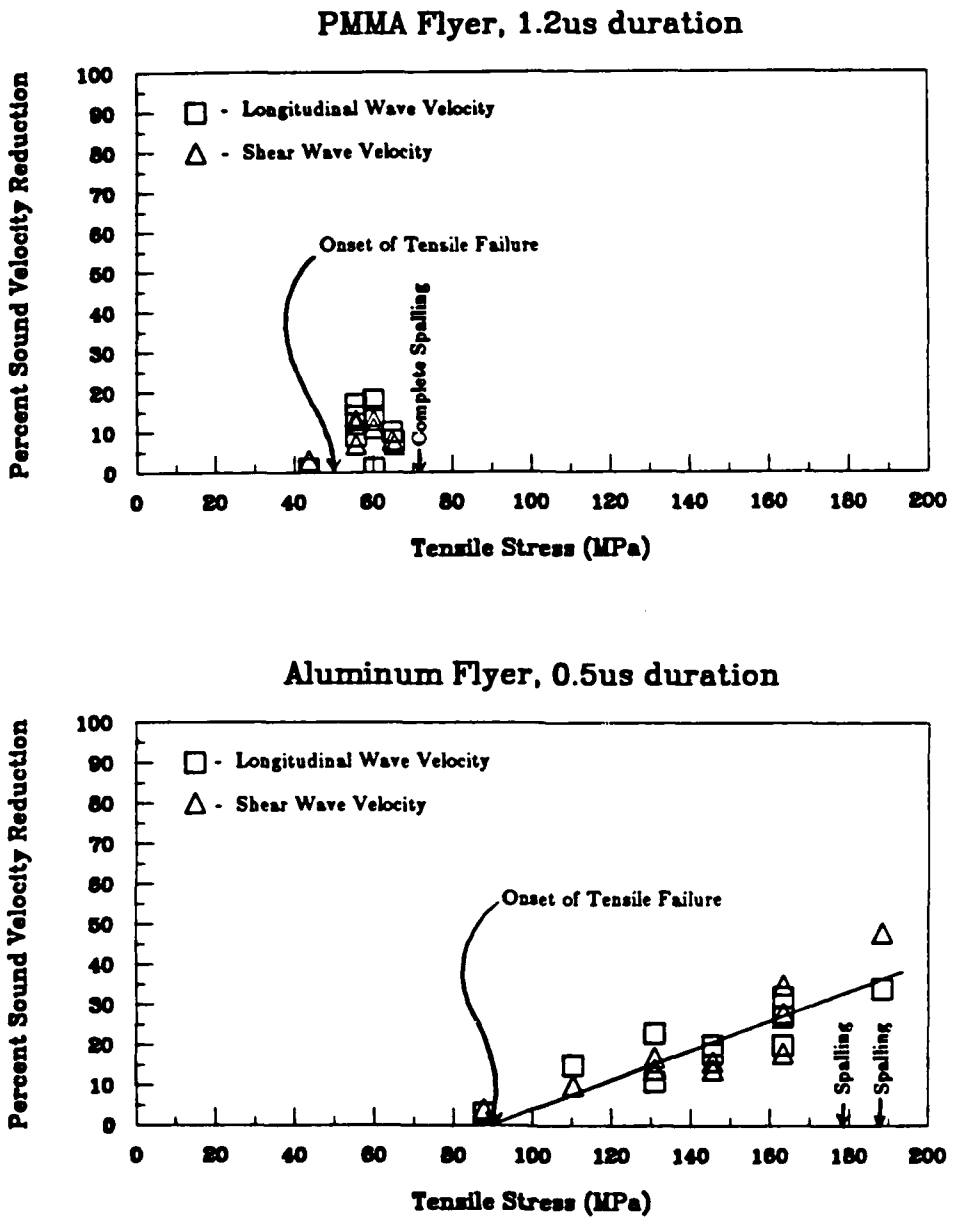

Figure 12. A new technique of employing the onset of sound velocity reduction to determine onset of dynamic tensile failure was tested. Bedford limestone specimens were tested following one-dimensional tensile experiments with 1.2 ms duration tensile pulse; B, 0.5 ms duration pulse. Considerably higher stresses are required for spalling in the shorter-duration experiments. Onset of tensile failure can be used to determine fracture toughness of rock.

(3) The percent reductions in longitudinal and shear wave velocities are approximately similar.

It has been known for some time that the tensile strengths measured at high strain rates can be considerably higher than those measured quasi-statically (Rinehart, 1965). This effect can be modeled in terms of fracture mechanics theory (Grady and Kipp, 1987). During quasi-static tests, assuming sufficient pre-existing microcracks that all orientations are represented, sample failure occurs when the stress σ is increased to the point that the largest crack can extend. This stress, σ, is such that the crack *stress-intensity factor*, K, equals the *fracture toughness* of the material, K_C. For a circular (penny-shaped) crack,

$$K = \frac{2}{\sqrt{\pi}} \sigma \sqrt{a} , \qquad (7)$$

where a is the crack half-length. Under dynamic loading conditions the criterion for crack propagation, that $K=K_C$, remains the same, but in the case of a suddenly-applied load, for early time $t < a/c_s$, K increases with time according to

$$K \cong \frac{2}{\sqrt{\pi}} \sigma \sqrt{c_s t} , \qquad (8)$$

where c_S is shear-wave velocity (essentially the effective crack length $c_S t$ increases with time). Thus a suddenly applied load can exceed the static strength of the material for $c_S t < a$ without producing failure. The greater the suddenly applied stress, the sooner $\sigma \sqrt{c_S t} = K_C$, and the sooner fractures will initiate.

If the stresses in the dynamic experiments are greater than the static strength of the material, so that $c_S t < a$, where a is now the largest inherent flaw size, eq. 8 can be used to compute the fracture toughness from the experimental data. In these short-duration experiments, failure will occur at stresses for which the value of K given by eq. 8 exceeds K_C, where t is the duration of the tensile stress pulse. The shear-wave velocity of intact Bedford limestone was determined to be 2.8 km/s. Assuming that the onset of crack extension produces a measurable reduction in the sample sound velocity, then crack extension first occurs at a stress of approximately 90 MPa for the 0.5 μs-duration experiments and 50 MPa for the 1.2 μs-duration experiments. Substitution then yields

$$K_c^{1.2\mu s} = \frac{2}{\sqrt{\pi}} 50 \sqrt{(2.8 \times 10^3)(1.2 \times 10^{-6})} = 3.3 \text{ MPa m}^{1/2}$$

$$K_c^{0.5\mu s} = \frac{2}{\sqrt{\pi}} 90 \sqrt{(2.8 \times 10^3)(0.5 \times 10^{-6})} = 3.8 \text{ MPa m}^{1/2}.$$

Thus the two experimental series provide a yield consistent value, 3.6±0.3MPa $m^{1/2}$, of the fracture toughness. This is a new, sensitive, way to determine the fracture toughness. This value is slightly higher than the range of 0.4 to 2.1 MPa $m^{1/2}$ reported under static conditions for 11 limestones by Atkinson and Meredith (1987). The cracks that are activated in each experiment are those whose half-lengths a are greater than $cs\ t$, or 3.4 mm for the 1.2 μs-duration experiments and 1.4 mm for the 0.5 μs-duration experiments. As the largest grains in Bedford limestone have half-lengths of about 1 mm, these theoretical crack lengths appear to be too great. This issue is discussed below.

At stresses higher than those producing the first cracking, cracking is initiated sooner (σ is larger so t is smaller in eq. 8), so cracks have more time to grow, and smaller cracks are activated ($c_S t$ is smaller in eq. 2), so presumably the activated flaws are spaced closer together. Complete tensile failure occurs at an applied stress that is sufficiently high that the density of activated cracks is sufficient for them to coalesce in the short duration

of the dynamic experiment. The tensile strengths were about 70 MPa for the 1.2 μs experiments and 180 MPa for the 0.5 μs experiments. Using fracture toughness values of 3.3 and 3.8 MPa $m^{1/2}$, this implies that cracks with half-lengths greater than 1.7 mm were activated after 0.62 μs in the 1.2 μs experiments, and that cracks with half lengths greater than 0.35 mm were activated after 0.12 μs in the 0.5 μs experiments. Once crack growth is initiated, propagation velocities are expected to be approximately one-third of the longitudinal sound velocity in the solid, determined to be 4.8 km/s for Bedford limestone. Thus, cracks could extend by about 1.0 mm (in each direction) from the 3.4 mm starter cracks in the remaining 0.6 μs of the 1.2 μs experiments, and 0.6 mm from the 0.7 mm starter cracks in the remaining 0.38 μs of the 0.5 μs experiments. The most straightforward interpretation of the dynamic tensile strength data is that 3.4 mm flaws are separated by about 5.4 mm, on average, and 0.7 mm flaws by about 1.9 mm, in Bedford limestone.

The samples of Bedford limestone studied have average grain sizes of about 0.5 mm, and the longest dimension of the largest grains is about 2 mm, so the distribution of 0.7 mm (full-length) cracks determined from the 0.5 μs experiments does not seem unreasonable. The large size of activated cracks calculated from the 1.2 μs experiments (6.8 mm at 50 MPa and 3.4 mm at 70 MPa) appear to be too large. However, they are large when calculated from static tensile tests of porous limestone and dolostone as well. For example, Gunsallus and Kulhawy (1984), performing parallel tests on 2 limestones, measured tensile strengths of 11.9 and 15.0 MPa, and fracture toughnesses of 1.36 and 2.06 MPa $m^{1/2}$. The largest inherent flaw sizes computed from eq. 1 for these two rocks are 2 cm and 3 cm, respectively. These are much larger than the grain sizes of the rocks and the latter is larger even than the size of the specimen used in the tensile tests. One possible explanation for this discrepancy is that in porous rock the interaction between neighboring flaws cannot be neglected when calculating K. One instructive model to consider is that of an infinite array of (two-dimensional) colinear cracks of equal

half-length a, with centers separated by equal distance b. In this case, under a uniform remote tension, K at the tip of each crack is greater than that for an isolated crack by a factor

$$\left(\frac{2b}{\pi a}\tan\frac{\pi a}{2b}\right)^{1/2} \qquad (9)$$

For cracks as far apart as they are long ($b = 2a$), this factor is only 1.13, but it is likely that in a porous rock it is those largest flaws or pores separated by the least distance (grain/grain contact areas) that grow first. For $b = 1.1a$, this factor is 2.2, and the computed inherent flaw size would be smaller by 2.2^2 or 4.9. Thus failure in a porous limestone at stresses at and moderately above the static tensile strength might require the interaction of several closely spaced pores. Alternatively, laboratory measurements of Kc using large artificial cracks might have to be modified when applied to grain size initial flaws (Ingraffen, 1987). Both of these possibilities would have important influences on dynamic tensile failure.

c. Conclusions

The observation that the longitudinal and shear-wave ultrasonic velocities are reduced by similar amounts in the recovered samples was unexpected. Induced spall cracks will preferentially grow parallel to the impact and rear surfaces of the sample (perpendicular to the direction in which the velocity is measured). Theoretical considerations suggest that aligned cracks should produce a greater reduction in longitudinal velocity than shear velocity, measured perpendicular to the crack planes (Anderson et al., 1974). Reductions in the longitudinal velocity of 20% are expected to be associated with reductions in shear velocity of perhaps 5% to 7%, smaller by a factor of 3 to 4, depending upon the precise values of crack density and aspect ratios. In contrast,

for randomly oriented cracks, a 20% reduction in longitudinal wave velocity is associated with about an 18% reduction in shear wave velocity (O'Connell and Budiansky, 1974), which is well within the scatter of the data. It is possible that the porous nature of the limestone contributes to scatter in induced crack orientation, particularly in view of the fact that for uniaxial tensile strain, stresses parallel to the sample faces will reach about one-third that perpendicular to the sample faces. Optical microscopy and velocity measurements parallel to the sample surfaces are required to investigate this further and will be carried out in the future.

REFERENCES

AHRENS, T. J., AND J. D. O'KEEFE, (1987). Impact on the Earth, ocean, and atmosphere. *International Journal of Impact Engineering*, **5**, 13-32.

ANDERSON, D.L., B. MINSTER, AND D. COLE, (1974). The effect of oriented cracks on seismic velocities. *J. Geophys. Res.*, **79**, 4011-4015.

ATKINSON, B.K., AND P.G. MEREDITH, (1987). The theory of subcritical crack growth with applications to minerals and rocks. *Fracture Mechanics of Rocks, ed. by B. K. Atkinson, Academic Press* , 111-166.

COHN, S.N, AND T.J. AHRENS, (1981). Dynamic tensile strengths of lunar rock types. *J. Geophys. Res.*, **86**, 1794-1802.

GLENN, L.A., (1976). The fracture of a glass half-space by projectile impact. *J. Mech. Phys. Sol.*, **24**, 93-106.

GRADY, D. E., AND M. E. KIPP, (1979). The micromechanics of impact fracture of rock. *International Journal of Rock Mechanics and Mining Sciences*, **16**, 293-302.

GRADY, D. E., AND M. E. KIPP, (1987). Dynamic rock fragmentation. *in: Fracture Mechanics of Rock, B. K. Atkinson, ed., Academic Press, London*, 534 pp..

GUNSALLUS, K. L., AND F. H. KULHAWY, (1984). A comparative evaluation of rock strength measures. *International Journal of Rock Mechanics and Mining Sciences*, **21**, 233-248.

HORAII, H., AND S. NEMAT-NASSER, (1986). Brittle failure in compression: Splitting, faulting, and brittle-ductile transition. *Philosophical Transactions of the Royal Society of London*, **319**, 337-374.

INGRAFFEN, A. R. (1987). Theory of crack initiation and propagation in rock, *in: Fracture Mechanics of Rock, B. K. Atkinson, ed., Academic Press, London* , 534 pp..

ISIDA, M., AND S. NEMAT-NASSER, (1987). On the mechanics of crack growth and its effects on the overall response of brittle porous solids. *Acta Metall.*, **35**, 2887-2898.

LANGE, M.A., T.J. AHRENS, AND M.B. BOSLOUGH, (1984). Impact cratering and spall fracture of gabbro. *Icarus*, **58**, 383-395.

MELOSH, H. J., (1984). Impact ejection, spallation, and the origin of meteorites. *Icarus*, **59**, 234-260.

O'CONNELL, R.J., AND B. BUDIANSKY, (1974). Seismic velocities in dry and saturated cracked solids. *J. Geophys. Res.*, **79**, 5412-5426.

RINEHART, J. S., (1965). Dynamic fracture strength of rocks. *Proceedings of the 7th Symposium on Rock Mechanics*, **1**, 205-208.

SAMMIS, C. G., AND M. F. ASHBY, (1986). The failure of brittle porous solids under compressive stress states. *Acta Metall.*, **34**, 511-526.

SHOCKEY, D. A., D. R. CURRAN, L. SEAMAN, J. T. ROSENBERG, AND C. F. PETERSON, (1974). Fragmentation of rock under dynamic loads. *International Journal of Rock Mechanics and Mining Sciences*, **11**, 303-317.

WALSH, J.B., (1965). The effect of cracks on the uniaxial elastic compression of rocks. *J. Geophys. Res.*, **70**, 399-411.

ACKNOWLEDGMENTS

We appreciate E. Gelle, M. Long, and W. Miller for technical assistance. We appreciate S. Yamada's efforts in assisting in report preparation.